JMEPEG (2011) 20:1157–1162
DOI: 10.1007/s11665-010-9632-2

1059-9495/$19.00

Synthesis of $SnFe_2O_4$ Nanomaterials Via High Energy Ball Milling of SnO (Stannous) and α-Fe_2O_3 (Hematite) Solid Precursors

Oswald N.C. Uwakweh, Rita Más, Carolyn Morales, Pedro Vargas, Josue Silva, Angel Rosa, Neshma Lopez, Richard Perez Moyet, and Yenny Cardona

(Submitted February 23, 2009; in revised form December 1, 2010)

The synthesis of single phase tin-ferrite, $SnFe_2O_4$, from tin (II) oxide or stannous oxide (SnO), and hematite (α-Fe_2O_3) solid precursors was carried out via high energy ball milling (HEBM) under wet condition involving the addition of controlled amounts of acetone. The stoichiometric amounts of the precursor materials were ball milled continuously for up to 22 h in a Spex-8000D mill using a ball-to-powder ratio of 40:1, with hardened stainless steel balls in WC-lined jars. The time-dependent formation of the $SnFe_2O_4$ based on combined X-ray diffraction and room temperature Mössbauer spectroscopy (MS) measurements revealed reaction enhancements associated with particles size reduction. The 22 h milled material indicated that synthesized $SnFe_2O_4$ had a particle size of 10.91 nm, coercivity of 4.44 mT, magnetic saturation/remanent ratio (M_r/M_s) of 0.085, while its superparamagnetic behavior was confirmed based on the combined MS and vibrating sample magnetometer measurements.

Keywords mechanosynthesis, Mössbauer spectroscopy, nanomaterial, superparamagnetism, tin-ferrite ($SnFe_2O_4$)

1. Introduction

Spinel-based ferrites are a group of ceramic materials that have a wide range of, and potential for diverse applications. They derive their name from the naturally occurring mineral $MgAl_2O_4$ that has a face-centered-cubic structure. They are generally represented or designated as AB_2O_4 with the A divalent cation distinguished from the B trivalent cation based on their location within the crystal lattice. They are related to the well known magnetite Fe_3O_4 which has been extensively studied. This ferrimagnetic material is sometimes represented as $FeO \cdot Fe_2O_3$ though not as a solid solution to reflect that it has both ferrous and ferric ions. This representation is the basis for which other known ferrites are generally identified as $MeO \cdot Fe_2O_3$ or $MeFe_2O_4$ where Me standing for Metal cation include such divalent ions as Co, Mg, Mn, Ni, Zn, etc.

Oswald N.C. Uwakweh, Department of Engineering Science and Materials, University of Puerto Rico-Mayagüez, P.O. Box 9044, Mayagüez, PR 00681-9044; **Rita Más** and **Carolyn Morales**, Department of Industrial Engineering, University of Puerto Rico-Mayagüez, P.O. Box 9016, Mayagüez, PR 00681-9016; **Pedro Vargas, Josue Silva,** and **Angel Rosa**, Department of Mechanical Engineering, University of Puerto Rico-Mayagüez, P.O. Box 9045, Mayagüez, PR 00681-9045; **Neshma Lopez**, Department of Chemical Engineering, University of Puerto Rico-Mayagüez, P.O. Box 9045, Mayagüez, PR 00681-9045; and **Richard Perez Moyet** and **Yenny Cardona**, Department of Physics, University of Puerto Rico-Mayagüez, P.O. Box 9016, Mayagüez, PR 00681-9016. Contact e-mail: uwakweh@ece.uprm.edu.

Their use and interest date back to more than four decades when their magnetic properties were studied and reported by Néel (Ref 1) who suggested that small antiferromagnetic particles can exhibit superparamagnetism and weak ferromagnetism due to uncompensated spins in the two sublattices. Apart from their bulk properties interests, these materials continue to be attractive because of the behaviors associated with their nanoscale structures. The unique properties of the nanoscale particles are associated with the adoption of the materials' crystal structure to a small size scale and their large surface-to-volume ratio. This makes it possible for the materials to exhibit properties that are not observed in their bulk forms, i.e., when average grain size is generally greater than 100 nm.

These ferrospinels are special magnetic materials whose importance is manifested on their uses in a host of scientific and technological applications such as in magnetic devices and switching devices (Ref 2-4) to mention, but a few. Taken together, they constitute a class of material with potentials or possible uses including but not limited to transformer cores, magnetic memories, biomedical applications, ferrofluids, and heterogeneous catalysts. Further, their performances are tied to their compositions with respect to cationic distribution, microstructures, which are related to their syntheses methods together with attendant processing history (Ref 5) employed in products fabrication.

Traditional routes in the syntheses of ceramics-based materials involve among other steps high-temperature reaction of precursor materials (Ref 6). Following high temperature syntheses, the resulting materials are often subjected to the action of mechanical milling with further or subsequent heat treatment (Ref 7-11). Within two decades or so, with the advent of intense use of high energy ball milling (HEBM) to generate mechanical alloying and nanomaterials in diverse materials systems such as metallic alloys (Ref 12-14), the technique has

since evolved from its use in generating nanosized particles (Ref 15-19), to its use in the syntheses of ceramic based materials in a process commonly referred to as mechanosyntheses (Ref 20-23). Mechanochemical processing entailing synthesis of MFe_2O_4 (M = Cu and Zn) spinel systems based on different milling procedures showed that different starting materials can be used to obtain ferrospinels with varying magnetic properties even when the final material had nearly identical phases (Ref 24, 25). Since these materials can be generated by substituting the Fe cations with other divalent metal ions in order to generate $MeFe_2O_4$ with the spinel structure from the parent Fe_3O_4, it is expected that possibility of newer ones can be investigated with appropriate cation doping. In this wise, the doping of Fe_3O_4 with Sn was reported by Drokin et al. (Ref 26) who investigated their photoconductivity behavior in polycrystalline states ($Sn_xFe_{3-x}O_4$, with $x = 0.1$, 0.2, 0.3, 0.4, and 1) while Berry and Helgason (Ref 27) studied the Sn doping of iron oxides with composition $Sn_{0.1}Fe_{2.9}O_4$ using Mössbauer spectroscopic techniques.

As is common in most ceramic syntheses, the Sn-doped ferrites were mainly prepared via solid-state reactions which entailed temperatures as high as 1300 °C over long-time periods with the realized polycrystalline materials having grains in the micrometer (μm) ranges. Independent of the solid-state reaction technique, Liu et al. (Ref 28) reported that they were able to successfully synthesize $SnFe_2O_4$ nanoparticles through solid-phase reaction in solution described as precipitation exchange. According to these authors, their synthesis method has an advantage over traditional solid-state reaction as relatively low temperature (around 100 °C), because of their simple experimental setup resulting in well-crystallized material. Using $FeCl_3 \cdot H_2O$, $SnCl_2 \cdot H_2O$, and $NH_3 \cdot H_2O$, as starting materials, they were able to synthesis $SnFe_2O_4$ with particle size control ranging from 4 to 15 nm after undertaking an open air tube furnace thermal anneal in the temperature range of 85 to 200 °C, respectively. Given that the overall interest in nanosized materials is based on the fact that their size-dependent properties confers on them a lot of technological premise, we undertook the synthesis of $SnFe_2O_4$ via HEBM-induced reaction of solid precursors at room temperatures. In this study, SnO oxide was mixed in stoichiometric amounts with α-Fe_2O_3 followed by the addition of controlled amounts of acetone in what we describe as wet ball milling synthesis. The resulting synthesized $SnFe_2O_4$ material was achieved by monitoring the ball milling process as a function of time. In order to monitor the mechanosynthesis process, sample materials were drawn intermittently as a function of time to determine the progress of the synthesis process, and subjected to X-ray diffraction (XRD), vibrating sample magnetometer (VSM), and Mössbauer spectroscopy (MS) measurements.

2. Experimental Procedure

Alfa Aesar supplied SnO, (tin(II) oxide) also known as stannous oxide, and iron(III) oxide (hematite), α-Fe_2O_3, powders having average grain size of 74 nm was ball milled with hardened stainless steel balls measuring 10 mm in diameter, in a WC-lined steel jars. The ball-to-mass ratio (BPR) used was 40:1, while the milling operations were all carried out under wet condition entailing the use of controlled amount of acetone (0.6 mL) that was added to the initial mixture before subsequent ball milling using a Spex-8000D mill. The size of the 17 hardened steel balls used was 10 mm. The milling times were varied from 5 to 22 h. Following ball milling, samples were drawn from the milled powders for the different characterization techniques used in this study.

A Joel 5410-LV scanning electron microscope operated at 10 kV was to undertake a scanning electron microscopy (SEM) characterization of the materials. Thus, the morphologies of the materials in their as-received and ball milled states were observed and compared.

The XRD was carried out with a Siemens D500 diffractometer with a CuK_α radiation source and a (β) Ni filter. The scanning range used in the measurements was 5° to 95° in 2θ by steps of 0.03° and operated with a current of 35 A and a voltage of 30 kV. The Power Cell program was used in the peaks analyses in order to determine the average crystallite size, residual strain, and lattice parameter changes accompanying the ball milling of the material.

The magnetic properties such as coercivity and saturation magnetization were determined through measurements conducted with a Lakeshore 7400 Series VSM, with applied field up to 22000 gauss on powder samples weighing about 30 mg.

The Mössbauer spectroscopic measurements were carried out with a WEBRES spectrometer (now SEECO Company) operating at constant acceleration mode with a 50 mCi ^{57}Co gamma ray source in Rh matrix made by Ritverc GmbH. The velocity range of the scan was selected in order to permit a thorough scan of the samples in order to reveal features associated with both the paramagnetic and magnetic portions of the recorded spectra. The 1,024 point raw data were folded and analyzed using WMOSS, a public domain Mössbauer spectral analysis program available at www.SEECo.us (Ref 29) which was formerly www.webres.com. The velocity calibration was carried out with known line positions of room temperature α-Fe metal.

3. Results and Discussion

3.1 Scanning Electron Microscopy

Figure 1(a) showed the SEM image of the mixture of SnO and α-Fe_2O_3 after 5 h of ball milling during the synthesis of $SnFe_2O_4$ material, while Fig. 1(b) and (c), showed the morphologies of the materials after 10, and 22 h respectively. Examination of Fig. 1(a) showed the material mixture existing in the form of clumps of particles having varied sizes. The bigger clumps showed well-defined facets which were not observed in the ball milled states after 10 and 22 h. Further, the 22 h ball milled material exhibited a lot of particle agglomeration and interparticle pores, in addition to crystallite size reduction as would be discussed further in the XRD section.

According to Anantharaman et al. (Ref 30), spinel ferrites have a preference for crystallographic surface exposure found to be the *B*(111) and *D*(110) planes based on the Knözinger and Ratnaswamy (Ref 31) notations. These surfaces have octahedral sites as opposed to the tetrahedral ones. According to these authors, all the other crystallographic planes associated with the AB_2O_4 spinel structure have the A and B types sites on their exposed surfaces except the *D*(110) and the *B*(111) type surfaces. In other to avoid possible confusion over the use of similar letters (*B* and *D*) for the surfaces and typical spinel structure, the spinel structure would henceforth be designated

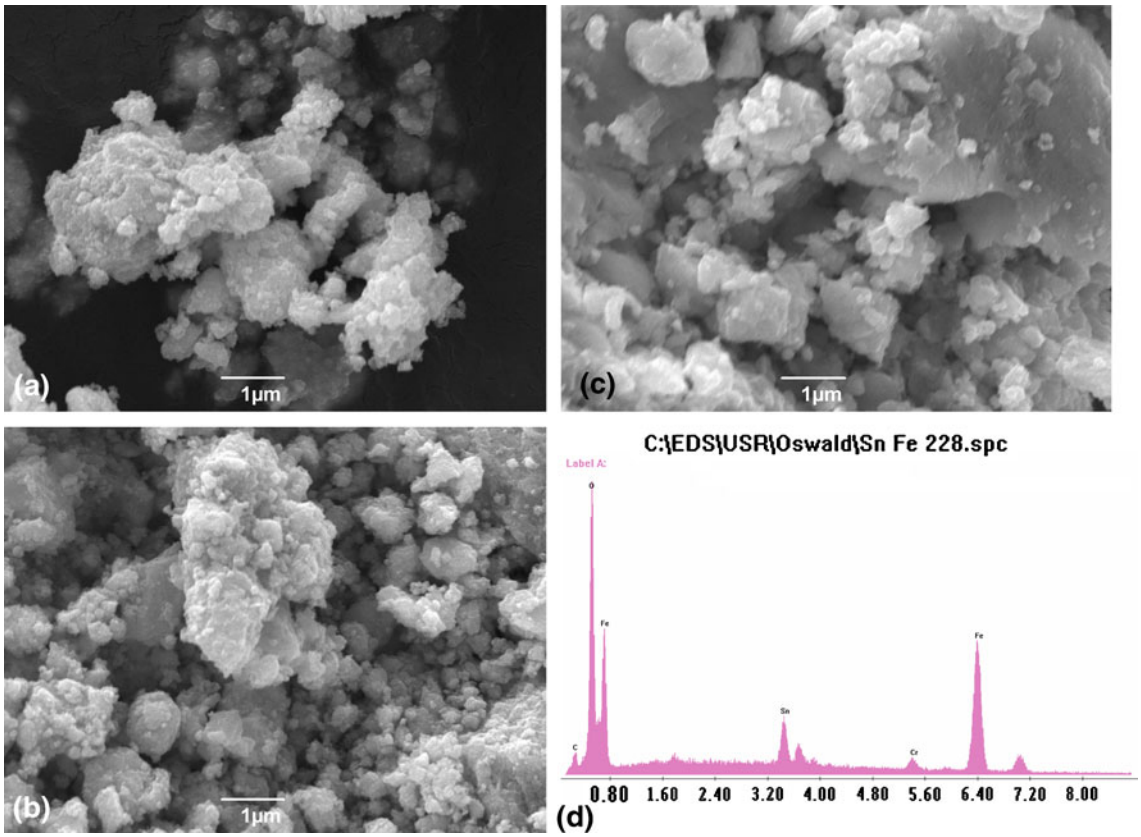

Fig. 1 SEM micrograph of (a) 5 h, (b) 10 h, and (c) 22 h ball milled SnO + α-Fe_2O_3 during the synthesis of $SnFe_2O_4$. (d) DAX spectrum showing elemental analysis of the ball milled state corresponding to 22 h

as $MeFe_2O_4$ where Me is the metal divalent cation in the spinel structure. In addition to these studies, others as well were in general agreement based on other spinel structured materials. For instance, Shelef and Yao (Ref 32) concluded that tetrahedral sites were not on the surface of spinel structured materials such as Co_3O_4 and were later backed by the studies of Beaufils and Barbaux based on their differential neutron diffraction studies on Co_3O_4 and $MgAl_2O_4$, that only the *D*(110) and *B*(111) planes are exposed on the surface (Ref 33-35). The morphologies corresponding to the different states of ball milling of this study suggested that the materials were in metastable states since the well-defined facets were not observed at the magnification used in this study. Further, as shown in Fig. 1(d), the EDAX spectrum of the material after 22 h of ball milling showed that the material was homogenous, and was as well at 5 h of ball milling. While some contamination may occur during ball milling, the homogeneity of the milled materials is usually not compromised.

3.2 X-Ray Diffraction Measurements

Powder XRD of the precursor materials, hematite (α-Fe_2O_3) and SnO in their as-received bulk forms were recorded and constituted the basis for comparison with the milled states. This was achieved by carrying out the XRD measurements on the manually mixed precursor materials as shown in Fig. 2(a) with characteristic peaks associated with the phases indicated with different symbols. Their indexing was based on the knowledge of the tetragonal crystal structure of SnO and the rhombohedral crystal structure of the α-Fe_2O_3 materials. In general, the

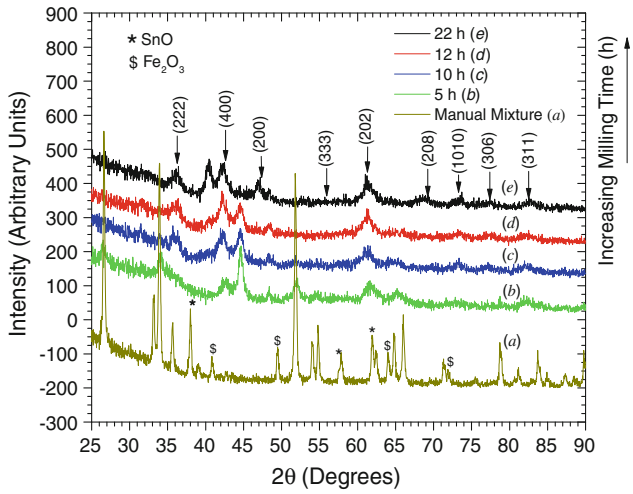

Fig. 2 XRD patterns corresponding to the different ball milled states, starting from the manual mixture of SnO and α-Fe_2O_3

intensities of the SnO peaks were much higher than those of hematite. The diffraction spectra shown in the Fig. 2(b-e), corresponding to the different ball milled states starting from 5 h in comparison to manual mixture spectra, indicated combinations of peaks loss of intensities, broadening, and shifts. These were evidence of both structural changes and progression of the synthesis of the single phase $SnFe_2O_4$. In addition to the peaks broadening, there were reductions in

peaks intensities that accompanied the shifts of the peaks after the reaction between the precursors had commenced. For instance, within the first 5 h of ball milling, the peaks corresponding to (104), (110), and (113) (around 2θ = 33°, 35.5°, and 41°, respectively) for α-Fe_2O_3, while, (101), (110), and (002) (around 2θ = 30°, 33°, and 37°, respectively) for the SnO, phases had reduced drastically in their intensities. Further, the peaks observed in the 2θ° = 30°-35°, and 2θ° = 50°-60°, ranges diminished and disappeared after 5 h of ball milling. Further, the emergence of the peaks corresponding to the new phase, $SnFe_2O_4$, manifested around 2θ° = 35°-47° range for instance, demonstrated the efficiency of the mechanosynthesis process. In addition to the gradual and progressive increase of intensities of this peak, the same trend was observed for the peaks in the 2θ° = 39°-44° range. After 22 h of ball milling, the emergence of the peaks around 2θ° = 68°, and 75° was observed as opposed to their absence in the 5, 10, and 12 h of ball milling under the stated wet ball milled conditions. The indexing of these peaks was matched based on the knowledge of spinel structured magnetite and known ferrospinels, including the comparison of the data reported by Lui et al. (Ref 28) for the $SnFe_2O_4$ synthesis via ion exchange solid-state precipitation, and also according to Li et al. (Ref 36).

The analyses of the XRD measurements with the powder cell program revealed that the lattice parameter for the single phase $SnFe_2O_4$ was 0.8434 nm for the 5 h ball milled state, while 0.8543 nm for the 22 h ball milled state. In addition, based on the Williamson-Hall method (Ref 37), the particle size and average internal strain were equally determined. This method is based on plotting the expression: $\beta\cos\theta = \kappa\lambda/D + \eta\sin\theta$ (with the first term as the *y*-axis, and the third term on the *x*-axis. In the expression, β, is the width of the peak corresponding to peak position θ, while *D*, λ, and η, are the crystallite size (coherent scattering length), the wavelength of the radiation, and the microstrain, respectively. The constant, κ has a value that is approximately, 0.9, but can be in the range of 0.80-1.39, from which the crystallite size and strains are deduced from the slope and intercepts of the plot. The particle size corresponding to the 5 and 22 h ball milled states were 19.11 and 10.91 nm, respectively. The average internal strain was observed to be dependent on the milled state, with the values for the 5 and 22 h ball milled states corresponding to 0.00190 and 0.00430 mm/mm, respectively. Taken altogether, the XRD measurements proved that synthesis of the desired $SnFe_2O_4$ single phase took place progressively with ball milling, thereby justifying the mechanosynthesis via ball milling route as a valid method for obtaining ferrospinel materials. In other words, the simultaneous particle size reduction of the precursor materials under the high-energy impacts with the balls facilitated the chemical reaction synthesis.

3.3 Vibrating Sample Magnetometer

The VSM measurements corresponding to the different states of ball milling at room temperature were reported in Fig. 3(a-d) to reflect their XRD homologues of Fig. 2(b-e), respectively. These plots showed that the hysteresis decreased with ball milling time during the mechanosynthesis of $SnFe_2O_4$ from the solid SnO and α-Fe_2O_3 precursor materials. The plots showed a consistent general trend associated with difficulty in the attainment of saturation, with decreasing saturation as a function of time. This can be explained from the fact that the particle sizes were in the nanometer ranges, and progressive formation of the single phase $SnFe_2O_4$ with time. The evolution

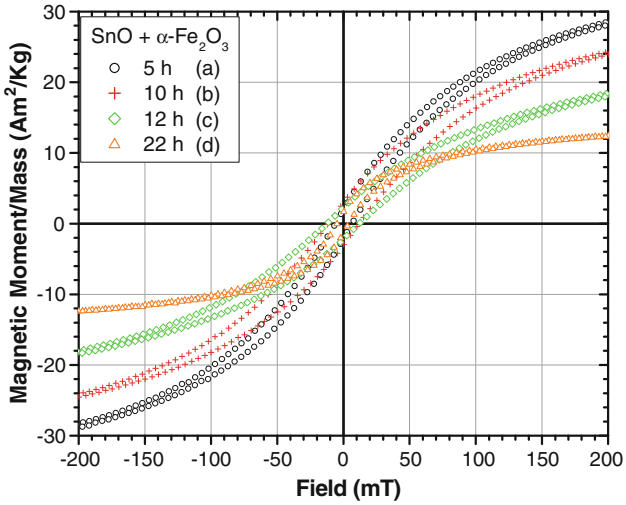

Fig. 3 VSM measurements of the synthesis of $SnFe_2O_4$ as a function of milling time: (a) 5 h, (b) 10 h, (c) 12 h, and (d) 22 h

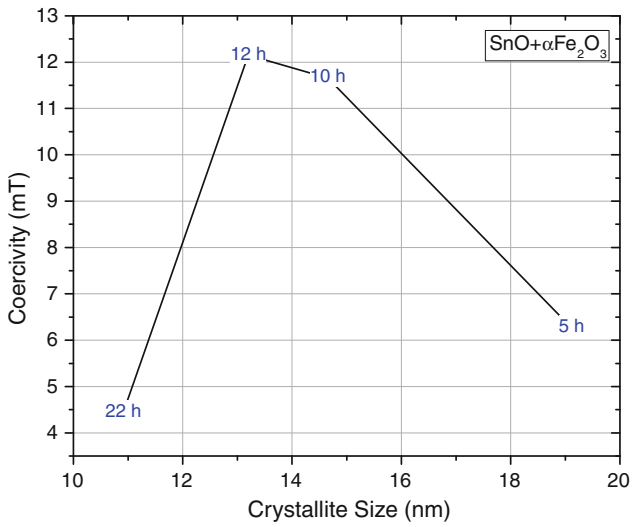

Fig. 4 Evolution of coercivity as a function of particle size of $SnFe_2O_4$ at different milling times from the solid SnO and α-Fe_2O_3 precursors

of the coercivity with particle size as shown in Fig. 4, indicated that in addition to the size of the particles, the metastable state of the milled material contributed to the observed coercivity. Thus, while the material was nanosized, its metastable state (with possible disorder) also played some role in determining its magnetic property.

As is well known, the magnetic anisotropic energy of nanoparticles are comparable to the energy of the thermal motion of the particle at room temperature, and so, the magnetization vector of the particle cannot be fixed along a certain direction and would become randomly oriented or fluctuate due to the thermal motion of the particles. The reduced hysteresis could be explained by the presence of anisotropic Fe spins inside nanoparticles as well as in their local environments. The substitution of Sn^{4+} in Fe_3O_4 introduces simultaneously an equivalent increase of the Fe^{2+} concentration which modifies strongly the magnetic properties. It has been reported that Sn

enters magnetite exclusively as Sn^{4+} into the octahedral sublattice according to Néel (Ref 38). The introduction of one Sn^{4+} ions into the B-sublattice would cause the disappearance of two Fe^{3+} ions via (i) direct replacement, and (ii) valency change from three into twofold.

The magnetic saturation decreased progressively with the 22 h ball milled material displaying the least value of 17.753 A m^2/kg and magnetic saturation and remanent ratio, M_r/M_s ratio of 0.0845. This is consistent with the fact that $SnFe_2O_4$ phase formed progressively with ball milling time, together with simultaneous structural changes such as cationic redistributions. Our results were consistent with the results of Liu and Li (Ref 39) who observed that the coercivity of $SnFe_2O_4$ synthesized via solid reaction in solution decreased with particle size reduction at ambient temperature. Though these authors attributed this behavior to the presence of noncolinear arrangements of Fe spins inside clusters and as well as in their local environments which caused decreased hysteresis, however, the drastic loss of coercivity in their sample with particles size of 4 nm at 350 K when particle agglomeration should have taken place suggested that other factors could have contributed to the coercivity loss. The overall coercivity of the milled material was 6.272 mT after 5 h of ball milling, while 4.441 mT corresponding to the 22 h ball milled state.

3.4 Mössbauer Spectroscopy Measurements

The corresponding room temperature Mössbauer spectroscopic measurements were carried out as a function of ball milling times are shown in Fig. 5(a, b, and c) corresponding the 5-, 10-, and 22 h of ball milled states respectively. The sextet peaks after 5 h of ball milling was due to some magnetically ordered particles. The intensities of the sextet peaks decreased as they became increasingly asymmetric with the progression of the ball milling process. At the same time, the central peaks increased in intensity while the doublet asymmetry became more prominent as reflected from the almost equal intensity of the doublet after 5 h of ball milling followed by their disproportionality after 10 and 22 h of ball milling, respectively. After 22 h of ball milling, the sextet peaks collapsed completely. These peaks were reflections of the single phase $SnFe_2O_4$ with nanometer size small enough to yield superparamagnetic behavior at room temperature. Thus, there was no effect of α-Fe_2O_3 particle size reduction contribution to the observed superparamagnetism since the XRD measurements revealed the complete reaction of the precursor's materials to the desired $SnFe_2O_4$ single phase. Similar or comparable progression of the synthesis process was observed for the α-Fe_2O_3 + MgO mechanosynthesis reported by Sepelák et al. (Ref 23). However, the synthesis of $SnFe_2O_4$ via precipitation exchange (solid phase reaction in solution) by Lui and Li (Ref 39) displayed Mössbauer spectra that were all nonmagnetic apparently because their samples were taken after the chemical reaction had taken place unlike our case where the progressive stages of the reaction were captured. The study of synthesis of $CoFe_2O_4$ via temperature-controlled coprecipitation by Kim et al. (Ref 40) showed that particle size distribution can equally generate mixture of superparamagnetic and non-superparamagnetic nanosized particles reflected on both XRD and Mössbauer spectroscopic measurements.

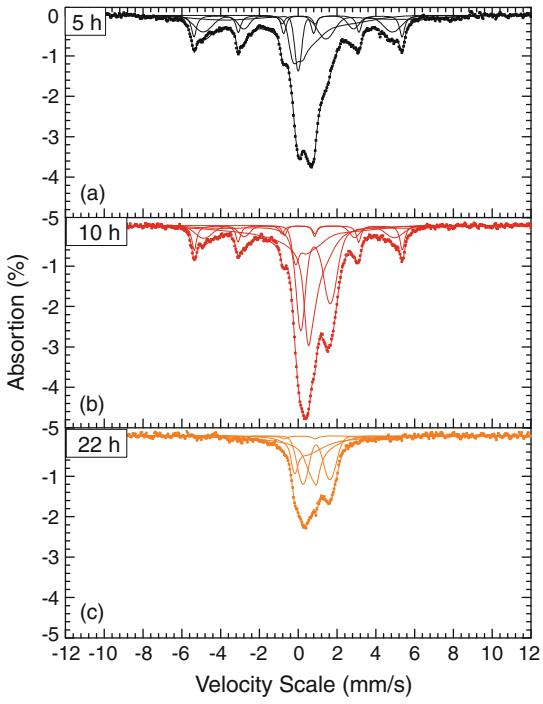

Fig. 5 Mössbauer Spectroscopy (MS) spectra of the synthesis of $SnFe_2O_4$ as a function of milling time: (a) 5 h, (b) 10 h, and (c) 22 h

4. Conclusions

The following conclusions could be drawn from the study of the synthesis of $SnFe_2O_4$ under wet conditions using HEBM of bulk crystalline precursor SnO and α-Fe_2O_3 solid materials at room temperature:

1. The formation of $SnFe_2O_4$ occurred progressively with increasing ball milling time. The synthesis process was accompanied by particle size reduction as evidenced by combined XRD, VSM, and Mössbauer spectroscopic measurements.
2. Continued ball milling resulted in complete synthesis of nanometer-sized particles. The lattice parameter of the formed $SnFe_2O_4$ particles changed with ball milling time, from 0.8434 to 0.8543 nm or (8.434 to 8.543 Å).
3. The hysteresis plots showed that mechanosynthesis was accompanied by particle size reductions attaining nanometer levels, while the coercivity and magnetic saturation decreased with the progressive formation of $SnFe_2O_4$ accompanied by structural changes such as cationic redistribution.
4. Mössbauer spectroscopy measurements showed that superparamagnetism arising from particle size reduction was exhibited by the particles after 5 h of ball milling, with the complete synthesis occurring after 22 h of ball milling.
5. Since there existed a critical particle size for superparamagnetic behavior, the decrease in magnetization saturation and relative ease associated with magnetization based on the initial slopes of the magnetization plots of the ball milled materials was consistent with the particle size deductions from XRD analyses.

Acknowledgment

The support of NSF-DMR PREM at UPRM based on Grant No. 0351449 for the authors is hereby acknowledged.

References

1. L. Néel, Superparamagnetisme de grains tres fins antiferromagnetiques, *C. R. Acad Sci.*, 1961, **252**, p 4075–4080 (Translated in Selected Works of L. Néel (Kurti, N., ed.), New York, Gordon and Breach, 1988, p 107–110)
2. R.W. Chantrell and K. O'Grady, The Magnetic Properties of Fine Particles, *Applied Magnetism*, C.D. Wright and G. Asti, Ed., Kluwer Academic Publishers, The Netherlands, 1994, p 113–164
3. T. Nakamura, T. Tsutaoka, and K. Hatakeyama, Frequency Dispersion of Permeability in Ferrite Composite Materials, *J. Magnet. Magnet. Mater.*, 1994, **138**(3), p 319–328
4. T. Tsutaoka, M. Ueshima, T. Tokunaga, T. Nakamura, and K. Hatakeyama, Frequency Dispersion and Temperature Variation of Complex Permeability of Ni-Zn Ferrite Composite Materials, *J. Appl. Phys.*, 1995, **78**, p 3983–3991
5. T.M. Clark and B.J. Evans, Enhanced Magnetization and Cation Distributions in Nanocrystalline $ZnFe_2O_4$: A Conversion Electron Mössbauer Spectroscopic Investigation, *IEEE Trans. Magnet.*, 1997, **33**(5 Part 2), p 3745–3747
6. J.A. Jacobs and T.F. Kilduff, *Engineering Materials Technology, Structures, Processing, Properties, and Selection*, 5th ed., Pearson Prentice Hall, USA, 2005
7. H.M. Yang, X.C. Zhang, A.D. Tang, and G.Z. Qui, Cobalt Ferrite Nanoparticles Prepared by Coprecipitation/Mechanochemical Treatment, *Chem. Lett.*, 2004, **33**, p 826–827
8. G. Ennas, G. Marongiu, S. Marras, and G. Piccaluga, Mechanochemical Route for the Synthesis of Cobalt Ferrite-Silica and Iron-Cobalt Alloy-Silica Nanocomposites, *J. Nanopart Res.*, 2004, **6**, p 99–105
9. S. Bid and S.K. Pradhan, Microstructure Characterization and Phase Transformation Kinetic study of mechanosynthesized Non-stoichiometric CdF_2O_4 by Rietveld's Analysis, *Jpn. J. Appl. Phys.*, 2004, **43**, p 5455–5464
10. M. Mozaffari and J. Amighian, Preparation of Al-Substituted Ni Ferrite Powders Via Mechanochemical Processing, *J. Magn. Mater.*, 2003, **260**, p 244–249
11. H.M. Widatallah and F.J. Berry, The Influence of Mechanica Milling and Subsequent Calcination on the Formation of Lithium Ferrites, *J. Solid State Chem.*, 2002, **164**, p 230–236
12. Z.T. Lui and O.N.C. Uwakweh, Ball Milling of Fe-Zn Intermetallics, *J. Mater. Res.*, 1996, **11**(7), p 1665–1672
13. Z. Lui and O.N.C. Uwakweh, Mossbauer Effect Study of Mechanically Alloyed Γ and Γ_1-Fe-Zn Intermediate Phases, *Metall. Mater. Trans. A*, 1997, **28 A**, p 743–747
14. O. Uwakweh, Z. Lui, A. Jordan, B. Chakoumakos, S. Spooner, and P. Maziasz, Neutron Diffraction and Phase Evolution of the Mechanically Alloyed Intermetallic Compound ς-FeZn, *Metall. Mater. Trans. A*, 2000, **31 A**, p 2739–2745
15. C.C. Koch, Mechanical Milling and Alloying, *Materials Science and Technology*, R.W. Cahn, P. Haasen, and E.J. Kramer, Ed., VCH Publishers, Weinheim, 1991, p 193–245
16. C. Suryanarayana, Mechanical Alloying, *Progr. Mater. Sci.*, 2001, 46, p 1–184
17. J. Ding, W.M. Miao, P.G. McCormick, and R. Street, High Magnetic Performance in Mechanically Alloyed Co-Substituted Fe_3O_4, *J. Appl. Phys. Lett.*, 1994, **65**(24), p 3135–3136
18. J. Ding, P.G. McCormick, and R. Street, Formation of Spinel Mn-Ferrrite During Mechanical Alloying, *J. Magn. Magn. Mater.*, 1997, **171**(3), p 309–314
19. N. Guigue-Millot, S. Begin-Colin, Y. Champion, M.J. Hytch, G. Le Caer, and P. Perriat, Control of Grain Size and Morphologies of Nanograined Ferrites by Adaptation of the Synthesis Route: Mechanosynthesis and Soft Chemistry, *J. Solid State Chem.*, 2003, **170**(1), p 30–38
20. V. Sepelák, U. Steinike, D.C. Uecker, S. Wissmann, and K.D. Becker, Structural Disorder in Mechanosynthesized Zinc Ferrite, *J. Solid State Chem.*, 1998, **135**(1), p 52–58
21. E. Avvakumov, M. Senna, and N. Kosova, *Soft Mechanochemical Synthesis: A Basis for New Chemical Technologies*, Kluwer Academic Publishers, Boston, 2001
22. T. Verdier, N. Nachbaur, and M. Jean, Mechanosynthesis of Zinc Ferrite in Hardened Steel Vials: Influence of ZnO on the Appearance of Fe(II), *J. Solid State Chem.*, 2005, **178**, p 3243–3250
23. V. Šepelák, A. Feldhoff, P. Heitjans, F. Krumeich, D. Menzel, F.J. Litterst, I. Bergmann, and K.D. Becker, Nonequilibrium Cation Distribution, Canted Spin Arrangement, and Enhanced Magnetization in Nanosized $MgFe_2O_4$ Prepared by a One-Step Mechanochemical Route, *Chem. Mater.*, 2006, 18, p 3057–3067
24. F. Goya and H.R. Rechenberg, On the Magnetic Properties of Mechanosynthesized and Ball Milled Spinel Ferrites, *Mater. Sci. Forum*, 2002, **403**, p 127–132
25. R.H. Kodama, S.A. Makhlouf, and A.E. Berkowitz, Finite Size Effects in Antiferromagnetic NiO Nanoparticles, *Phys. Rev. Lett.*, 1997, **79**(7), p 1393–1396
26. N.A. Drokin, E. Yu Aksenova, and Yu.A. Mamalui, Photoconductivity in Tin-Doped Magnetite, *Soviet Phys. Solid State*, 1984, **26**, p 1837–1838
27. F.J. Berry and Ö. Helgason, Mossbauer Spectroscopic Properties of Tin-Doped Iron Oxides, *Hyperfine Interact.*, 2000, **126**(1–4), p 269–275
28. F. Liu, T. Li, and H. Zheng, Structure and Magnetic Properties of $SnFe_2O_4$ Nanoparticles, *Phys. Lett. A*, 2004, **323**, p 305–309
29. Available at www.SEECO.us
30. M.R. Anantharaman, S. Reijne, J.P. Jacobs, H.H. Brongersma, R.H.H. Smits, and K. Seshan, Preferential Exposure of Certain Crystallographic Planes on the Surface of Spinel Ferrites: A Study by LEIS on Polycrystalline Spinel Ferrite Surfaces, *J. Mater. Sci.*, 1999, **34**, p P4279–P4283
31. H. Knözinger and P. Ratnaswamy, Catalytic Aluminas: Surface Models and Characterization of Surface Sites, *Catal. Rev.*, 1978, **17**(1), p 31–70
32. M. Shelef, M.A.Z. Wheeler, and H.C. Yao, Ion Scattering Spectra from Spinel Surfaces, *Surf. Sci.*, 1975, **47**, p 697–703
33. H.C. Yao and M. Shelef, Nitric Oxide and Carbon Monoxide Chemisorption on Cobalt-Containing Spinels, *J. Phys. Chem.*, 1974, **78**(24), p 2490–2496
34. J.P. Beaufils and J. Barbaux, Determination, Par Diffraction Differentielle de Neutrons, des Faces Cristallines Exposees par des Supports de Catalyseurs en Poudre, *J. Chim. Phys.*, 1981, **78**, p 347–352
35. J.P. Beaufils and J. Barbaux, Study of Adsorption on Powders by Surface Differential Diffraction Measurements. Argon on Co_3O_4, *J. Appl. Cryst.*, 1982, **15**, p 301–307
36. F. Li, H. Wang, L. Wang, and J. Wang, Magnetic Properties of $ZnFe_2O_4$ Nanoparticles Produced by a Low-Temperature Solid State Reaction Method, *J. Magn. Magn. Mater.*, 2007, **309**(2), p 295–299
37. B.D. Culity and S.R. Stock, *Elements of X-ray Diffraction*, 3rd ed., Prentice Hall, USA, 2001
38. L. Néel, Some Theoretical Aspects of Rock Magnetism, *Adv. Phys.*, 1955, **4**, p 191–243
39. F.X. Liu and T.Z. Li, Synthesis and Magnetic Properties of $SnFe_2O_4$ Nanoparticles, *Mat. Lett.*, 2005, **59**(2–3), p 194–196
40. Y. Kim, II, D. Kim, and C.S. Lee, Synthesis and Characterization of $CoFe_2O_4$ Magnetic Nanoparticles Prepared by Low Temperature-Controlled Coprecipitation Method, *Physica B*, 2003, **337**(1–4), p 42–51